Supporting Information

Kinetic switching between two modes of bisurea surfactant self-assembly

*Matthijn R. J. Vos,[a,b] Philippe E.L.G. Leclère,[c,d] Hugo Meekes, Elias Vlieg,[e] Roeland J. M. Nolte,[e] Nico A. J. M. Sommerdijk[*a]*

[a] *Laboratory of Materials and Interface Chemistry and Soft Matter Cryo-TEM Research Unit, Eindhoven University of Technology, Eindhoven Netherlands. Fax: +31 40 245 1036; Tel.: +31 40 247 5870; E-mail: n.sommerdijk@tue.nl.*

[b] *FEI Company, Achtseweg Noord 5, 5600 KA Eindhoven*

[c] *University of Mons (UMons), Laboratory for Chemistry of Novel Materials Center for Innovation and Research in Materials and Polymers (CIRMAP) Place du Parc, 20 B - 7000 Mons, Belgium. Ph.L. is Research Associate from FRS-FNRS (Belgium)*

[d] *Institute for Complex Molecular Systems,, Eindhoven University of Technology, P.O. Box 513, 5600 MB Eindhoven The Netherlands.*

[e] *Radboud University Nijmegen, Institute for Molecules and Materials, Heyendaalseweg 135, 6525 AJ Nijmegen.*

MATERIALS AND METHODS

General materials and equipment. The synthesis of surfactant **1** is described in the supplementary information. All reagents were obtained from Sigma-Aldrich and used without further purification. All solvents were purchased from Acros Chemica or Sigma-Aldrich and were of analytical quality (p.a.). The water used during synthesis was demineralised prior to use. Ultra pure water (Barnstead EASYpure LF system; R >17.7 MΩ-cm) was used for preparing the aggregates solutions. Transmission electron microscopy measurements were performed on a FEI Tecnai 20, type Sphera TEM equipped with a LaB6 filament operating at 200 kV. Images were recorded with a bottom mounted 1k x 1k Gatan CCD camera. A Gatan cryo-holder operating at ~ -170 °C was used for the cryo-TEM measurements. The sample vitrification procedure was carried out using an automated vitrification robot (FEI Vitrobot™ Mark III). TEM grids, both 200 mesh carbon coated copper grids and R2/2 Quantifoil Jena grids were purchased from Aurion. The Quantifoil grids were surface plasma treated using a Cressington 208 carbon coater operating at 5 mA for 40 seconds prior to the vitrification procedure. AFM images were recorded on a Veeco Multimode instrument equipped with a Nanoscope IV control unit using Nanosensors tips with resonance frequencies of 300 kHz operating in the tapping mode regime. For the in-situ AFM measurements the scanner was fitted with a heating stage and/or fluid cell.

Aggregate sample preparation.

In general, surfactant **1** was suspended at the desired concentration in ultra pure water and heated up to 100 °C resulting in a clear solution. The solution was then cooled to the desired formation temperature either in a controlled fashion or by cooling on the bench top, resulting in a turbid suspension or gel depending on the concentration of surfactant.

For the controlled crystallization experiments, the boiling 0.25 mg/mL surfactant solution was prepared in a closed vial and placed in a dessicator, which was situated in a stove operating at 90 °C and contained water to prevent evaporation of the surfactant solution. After 45 min. equilibration, the temperature was decreased gradually in a controlled way during a 1000 min. countdown to the desired temperature of formation. When the formation temperature was reached, the sample was left for a

growth period of 1 week, after which samples were taken for AFM and TEM measurements. For aged samples the growth period was extended for a longer time period of 4 months. This method was also used for shorter growth periods down to 1 day. For growth periods within the hour range, an oil bath was used to control the temperature of formation. In those cases a boiling surfactant solution was prepared in a closed vial and placed directly in an oil bath at the desired formation temperature. Samples for AFM and TEM were prepared after 1 or 2 h. The solutions were immediately deposited on the substrate for measuring AFM and TEM. This substrate was placed on a heater at the same temperature as the solution and rapidly blotted.

Transmission electron microscopy

For conventional TEM, small aliquots (3 μL) of the sampled aqueous ribbon suspension were applied to a 200 mesh carbon coated copper grid. The solutions were immediately deposited on the substrate for measuring TEM. The TEM-grid was placed on a heater at the same temperature as the solution and rapidly blotted. The samples were analyzed on the Sphera microscope at 200 kV and room temperature.

For cryo-TEM, images of the ribbons were obtained by applying small aliquots (3 μL) of the aqueous ribbon suspension at various concentrations to Quantifoil grids (R2/2 Quantifoil Jena) within the environmental chamber (relative humidity 100%) of the Vitrobot™ instrument at 22 °C. Excess liquid was blotted away with filter paper using an automatic blotting device within the environmental chamber of the Vitrobot™. The grid was subsequently shot through a shutter into melting ethane placed just outside the environmental chamber.[1] The vitrified specimens were stored under liquid nitrogen and observed at -170°C (Gatan cryo-holder) in the Sphera microscope. Micrographs were taken at 200 kV using low dose conditions.
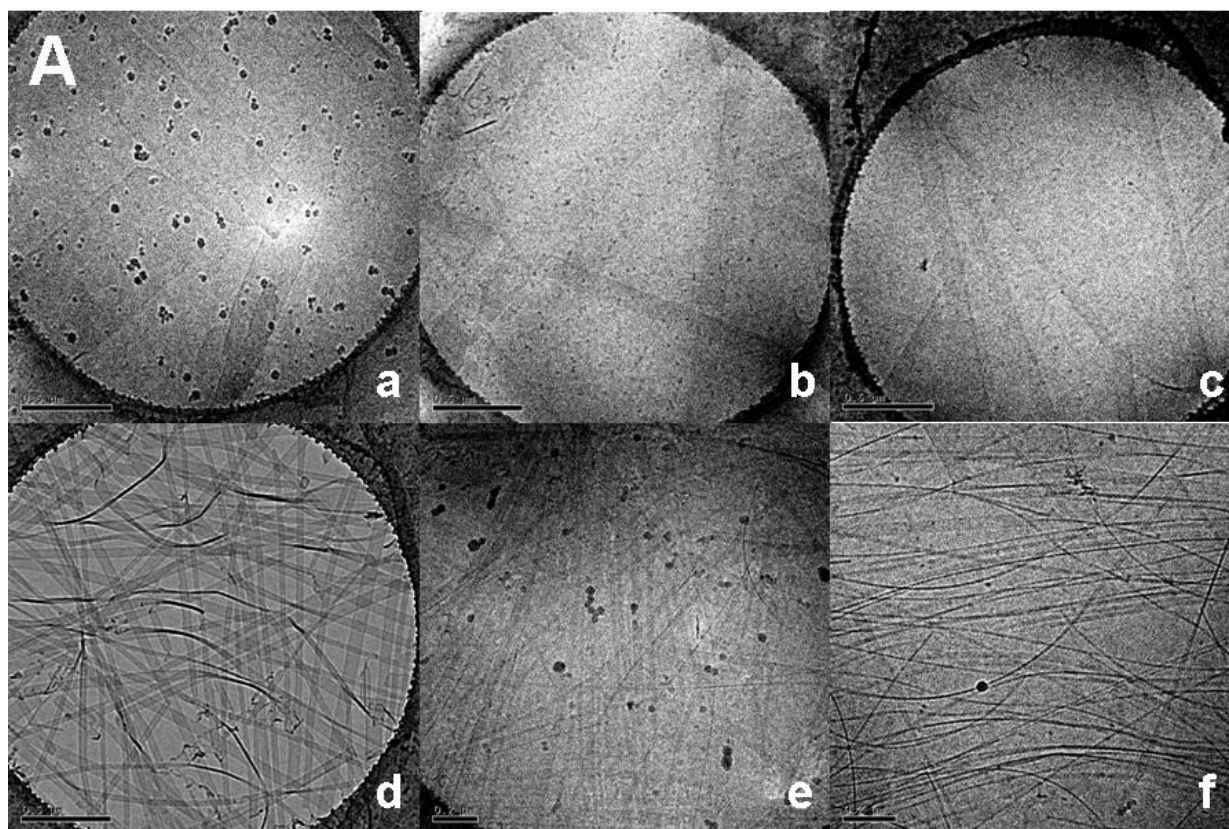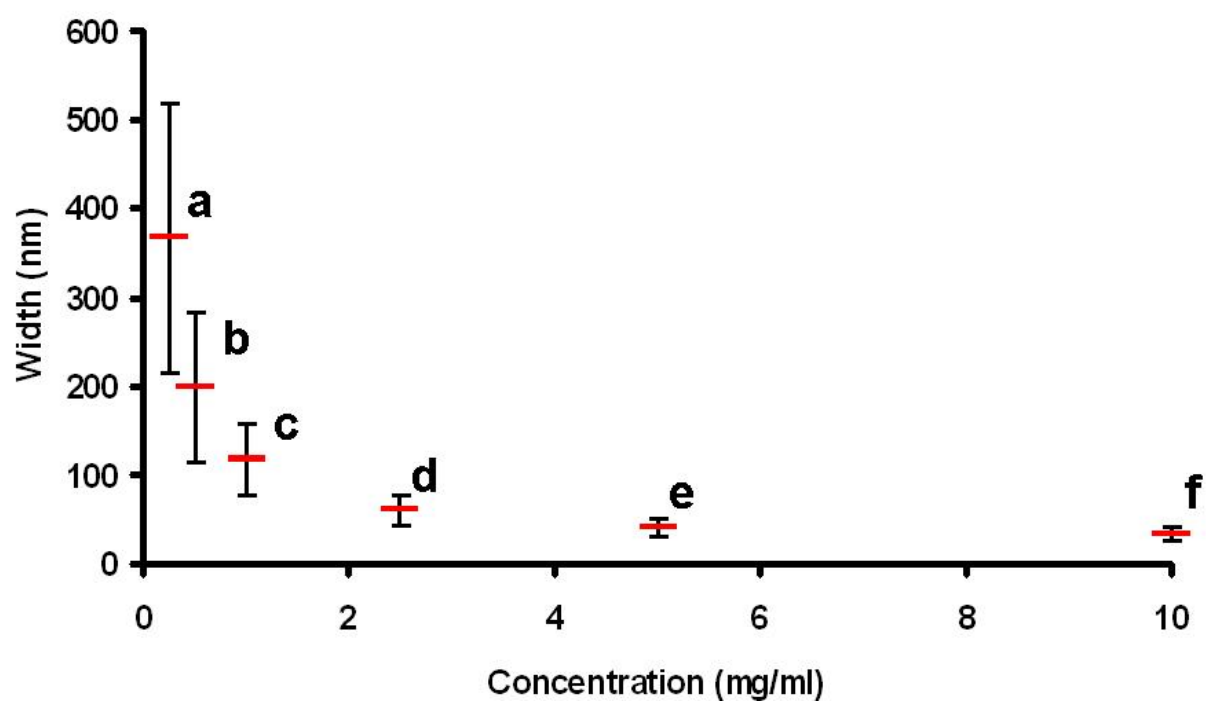
Figure S1. Extended version of Figure 1A from the main article text. **A.** Representative cryo-TEM

images of the decreasing ribbon width versus the increasing surfactant concentration (0.25, 0.5, 1.0, 2.5,

5.0, 10.0 mg/mL); scale bars: a-d 500 nm, e-f 200 nm. **B.** Plot of the ribbon width vs. the concentration. For each concentration N>100.

Atomic force microscopy

The samples for the crystallization experiments at different formation temperatures were prepared by drop casting of the aggregate suspension directly from the temperature controlled vial onto a clean glass slide, immediately followed by rapid removal of excess fluid using a stream of nitrogen.

For AFM measurements using the fluid cell and temperature control unit, a 1 mg/mL ribbon suspension was deposited on a glass slide as described above and placed in the fluid cell fitted with the temperature control unit. The temperature was slowly raised from room temperature to 80 °C and an AFM image was recorded every 10 °C in the dry state. A new similar sample was placed in the fluid cell and imaged before and after addition of demineralized water. A single ribbon was selected, subsequently the temperature was raised again slowly from room temperature to 80 °C and an image was recorded every 10 °C.

SYNTHESIS OF SURFACTANT **1**.
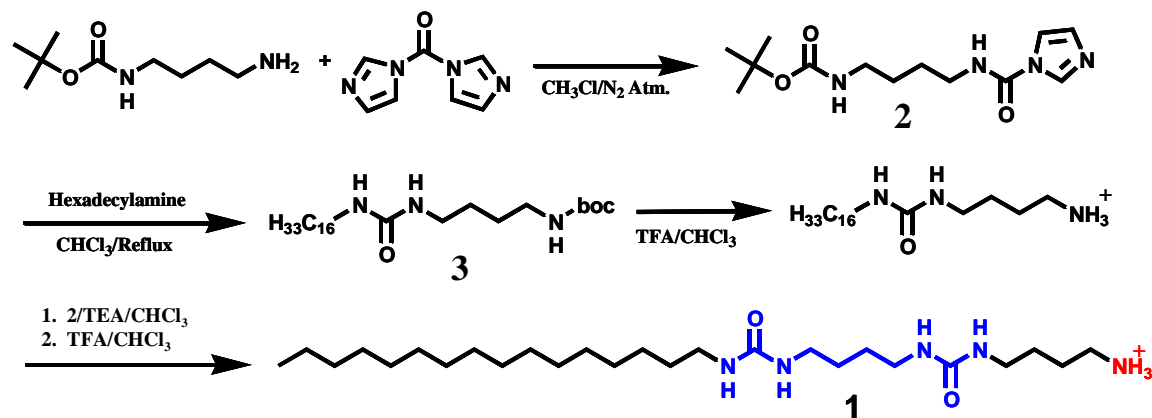
Scheme S1. Reaction scheme of the synthesis of surfactant **1** using CDI chemistry.

4[4(Hexadecylureido)butyl]ureido-butylammonium trifluoroacetate (1). Mono(*N*-boc)-1,4-butanediamine (34.8 g, 0.185 mol, Mw: 188.27) was dissolved in 120 mL of chloroform, after which

41.71 g (0.257 mol, Mw: 162.15) of carbonyldiimidazole (CDI) was slowly added. The mixture was stirred for 3 h. at 0 °C under a nitrogen atmosphere. The resulting product (**2**) was dissolved in 750 mL chloroform and washed with 400 mL water, 500 mL brine and dried over magnesiumsulfate. After filtration, the solvent was evaporated and 25.82 g (0.091 mol, Mw: 282.34) of **2** was dissolved together with 20.34 g (0.084 mol, Mw: 241.45) of 1-hexadecylamine in 300 mL of chloroform and refluxed for 3 h. After solvent evaporation, the product (**3**) was recrystallized using 450 mL methanol. Compound **3** was dried in a vacuum oven at 60 °C for 2 days to remove all traces of methanol. The Boc-protecting group was removed by slowly dissolving **3** in a mixture of 100 mL TFA and 200 mL chloroform and refluxed overnight, after which the solvent was removed and the remaining product was freeze-dried form glacial acetic acid. The resulting white powder (27.54 g, 0.059 mol, Mw: 469.63) was dissolved in 250 mL of chloroform together with 16.56 g (0.057 mol, Mw: 282.34) of compound **2** and 1 equivalent of TEA to remove the TFA counter ion, and left to reflux for two days while stirring vigorously. Subsequently, the solvent was evaporated and the product was purified via Soxlet extraction with hot methanol over the course of 1 week. After cooling the product recrystallized from the extracted methanol. The Boc-group of the resulting 17.2 g (0.03 mol, Mw 569.86) pure product was deprotected by dissolving the latter in a mixture of 136 mL TFA and 100 mL chloroform, which was subsequently refluxed overnight while stirring. After evaporation of the solvent the product was freeze-dried from glacial acetic acid to yield the desired pure product **1** as a white fluffy powder (16.97 g, 0.029 mol, Mw 583.77) in an overall yield of 34.4%. ^{1}H NMR (CDCl$_3$/CD$_3$OD): δ 0.9 (CH$_2$C*H*$_3$, 3H, t); 1.2-1.9 ((C*H*$_2$)$_{14}$CH$_3$, 28H, NHCH$_2$(C*H*$_2$)$_2$CH$_2$NH, 8H m); 2.9 (C*H*$_2$NH$_3$, 2H, m); 3.1 (C*H*$_2$NH, 8H, m); NH not visible due to H-D exchange. IR (ATR): ν = 3320 (NH) 2920, 2847 (*a-sym, sym*-CH stretch), 1660 (C=O TFA), 1613 (C=O Urea), 1569 (Amid II), 1478, 1465 (split CH$_2$ deform.). MALDI-TOF-MS: m/e 470.44 (M$^+$); 492.25 (M$^+$ -H + Na). Anal.calcd. (%) for C$_{28}$H$_{56}$F$_3$N$_5$O$_4$: C 57.6, H 9.7, N 12.0; Found (%): C 57.4, H 9.6, N 11.6.

X-RAY DIFFRACTION STUDIES
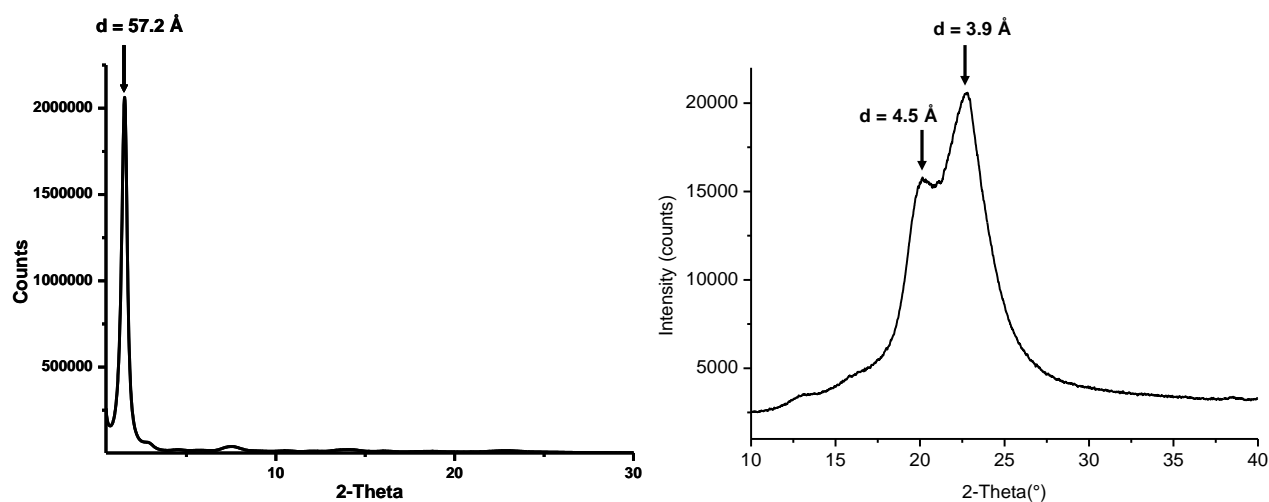
Figure S2. Grazing incident XRD on horizontally deposited ribbons showing a large first order peak at 57 Å corresponding to the ~6 nm thickness of the ribbons measured with AFM and TEM (left). X-ray powder diffraction (XRPD) on a dried gelled concentrated ribbon sample of **1** at 40 mg/ml surfactant concentration, showing 2 main first order reflections at 4.5 Å and 3.9 Å, corresponding to the hydrogen bond distance in the length direction and the packing distance of the hydrocarbon tails, respectively (right).

The original assignment of d-spacings previously made on the basis of combined polarized IR and grazing incidence X-ray diffraction studies is now refined using additional XRPD measurements on a more concentrated sample (40 mg/ml) (Fig S2) and molecular modeling. These measurements showed two first order reflections at 3.9 Å and 4.5 Å.[2] Using molecular models, these data were found to fit with minimal overlap of the Vanderwaals-radii, to a 2D crystal structure in which the 3.9 Å d-spacing makes an angle of 125° with respect to the 4.5 Å spacing. This results in two molecule-to-molecule distances, i.e. 4.76 Å and 5.4 Å, with the former distance corresponding well to H-bond distances commonly found for bis-urea based systems.[3] The resulting model (Fig. S3) shows a densely packed array of molecules

interconnected by H-bonds along the long y-axis of the ribbon with their hydrocarbon chains interdigitated pointing alternatingly up and down along the x-direction, forming a 2D crystal-like structure with an elongated hexagonal pattern.
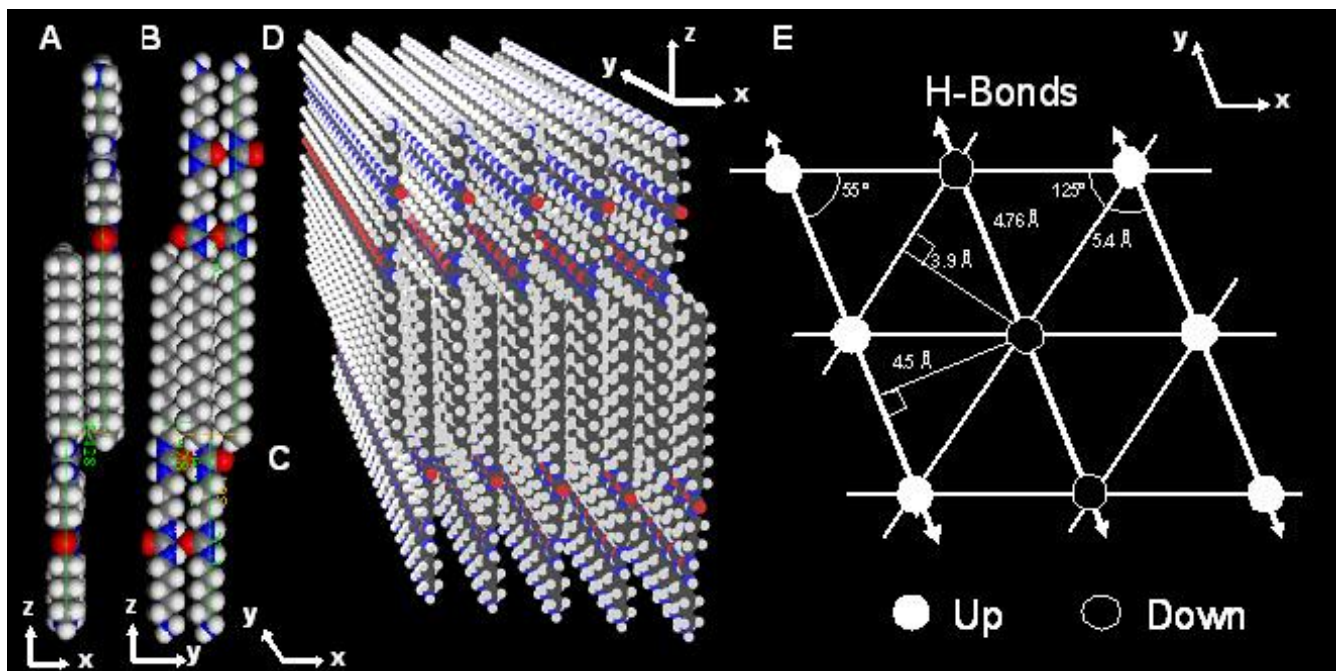
Figure S3. Close Packed molecular model constructed using the Materials Studio Software. **A.** Side view of the proposed unit-cell along the y-direction. **B.** Same as **A** along the x-direction. **C.** Top view of **A** along the z-direction. **D.** Projection of a 3D POV-Ray image of the proposed molecular packing within the ribbon structure. **E.** Proposed 2D crystal lattice of the ribbon aggregate along the z-axis. Solid spheres are head groups pointing up whereas open spheres are pointing down. The arrows along identical spheres indicate the hydrogen-bond direction.

VARIABLE TEMPERATURE –ATOMIC FORCE MICROSCOPY
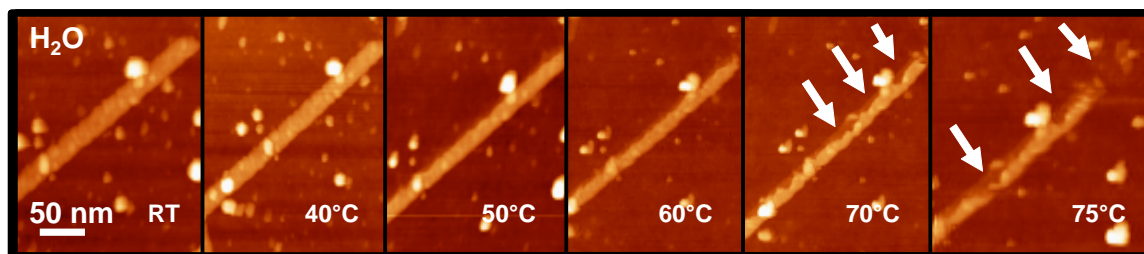
Figure S4. In situ AFM images measured in a fluid cell showing dissolution of a single ribbon above 70° C as indicated by the white arrows.

Variable temperature (VT) *in situ* AFM measurements (Fig. S4) both in water and in the dry state showed that upon heating to 70 °C the ribbons disintegrated. This is in line with the visual inspection of a turbid ribbon solution, which upon heating to 70 °C turns clear, also indicating the dissolution of the aggregates. The turbid suspension was regained upon cooling below 70 °C, indicating reformation of the ribbon aggregates, which was confirmed by AFM and TEM. Therefore the formation temperature of the aggregates can be set at 70 °C.

VARIABLE TEMPERATURE INFRARED
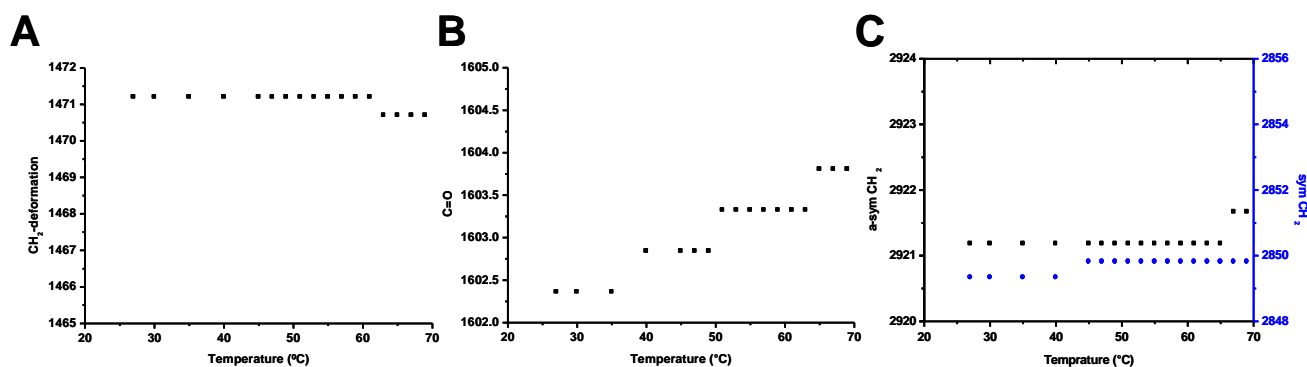
Figure S5. IR peak shifts vs. temperature. All spectra did not show any significant changes indicating a similar molecular packing over the total temperature range. **A.** CH_2-deformation band remains in an all-*trans* state (1471 cm^{-1}). **B.** Carbonyl C=O stretch shifts only marginal, however the peak position at low wavenumbers (~1604 cm^{-1}) still indicates strong H-bonding. **C.** No significant change in the CH_2 a-symmetric and symmetric stretch vibration.

EQUIPMENT

^{1}H-NMR spectra were recorded on a Varian Mercury 400 MHz instrument. Elemental analysis was performed on a Perkin Elmer 2400 apparatus. The VT-IR measurements were recorded using a Bio-Rad

Excalibur IR spectrophotometer equipped with a Specac Golden Gate ATR Unit fitted with a diamond window and operating with a 2 cm^{-1} resolution. The VT-IR experiments were carried out with deuterated water as solvent to avoid overlap of the carbonyl vibration with the H_2O signal. Powder X-ray diffraction measurements were carried out on a Rigaku Powder diffractometer (Cu-tube: $CuK\alpha_1$ radiation; λ=1.54056Å, 40 kV, 30 mA). Gracing incidence X-ray Diffraction was measured on a Bruker D8 Advance instrument ($CuK\alpha_1$ radiation) equipped with a Vantec detector.

Analysis of facet formation in surfactant assemblies

The controlled growth of aggregates was performed using 0.25 mg/ml surfactant solution which was prepared above the formation temperature in a closed vial by heating to 90 °C. Subsequently, the aggregates were allowed to grow by keeping the solution at 65 °C for 1 week. AFM and TEM showed the formation of faceted 6 nm thick crystal-like aggregates whose average aspect ratio was 2.5 (Figure S6B); a dramatic decrease compared to the ribbons grown at room temperature (a.r. >50) (Figure S6A). Irrespectively of their size almost all of these aggregates showed faceted top ends with an average top angle of 125 degrees (N=80) reflecting their organization on a molecular level (Figure S6C).

Close examination of many top ends from ribbons grown at RT revealed slanted, rounded, fragmented and unfinished ends (Figure S7A/B). These indicate that the change in top end morphology from faceted to flat is not likely to be related to the formation of a different facet type with a 90 degree angle[4] (Figure S6C) and are indicative of roughening effects as found frequently for 3D crystals at higher supersaturation levels. Since thermal roughening is related to an increase in the entropy term as a consequence of the temperature being increased ($\Delta G = \Delta H - T\Delta S$), the formation of roughened ends in this case, i.e. with decreasing temperature, cannot be assigned to such a process. The disappearance of faceted ends as a result of increasing supersaturation, therefore must be the result of kinetic roughening.[5] In addition, it has been shown that transport-limited crystal growth can cause a second roughening effect: the formation of dendritic and dagger-shaped structures.[6] More precisely, when the growth rate of a crystal plane exceeds the rate of transport of molecules to the crystal surface, no stable facets can be

developed and the plane will grow in the direction in which free molecules are still available, resulting in needle-like or dendritic outgrowths.[7] These structural features could also be found, although not frequently, in samples grown at temperatures below 55 °C (Figure S7C/D), highlighting again that variation in the observed morphological features can be explained using crystal growth mechanisms.

Although faceted top ends are observed at lower supersaturation, aging of the ribbon morphology with roughened top ends in their mother liquor does not lead to the development of facets in time. The analysis of the crystal-like aggregates at different time points showed that the aspect ratios present at the early points in growth remained unchanged, only a smoothing of the end faces was observed. These results indicate that the exchange of molecules between the aggregates and the solution in the exhausted mother liquor has become extremely slow. Since the crystal-like morphology formed at low supersaturation levels at early time points is nearer to the final faceted morphology, aging of these aggregates did show the formation of better defined facets in the investigated time period (~4 months). The roughened ends of the ribbon morphology formed at lower supersaturation presumably need much more time to develop facets.
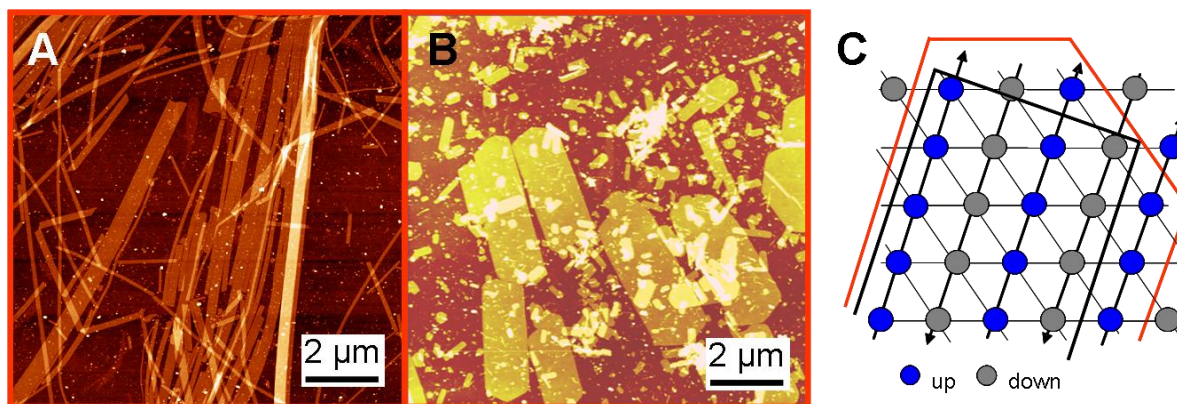
Figure S6. A. AFM image of ribbon aggregates grown at r.t. (1 mg/mL). **B.** AFM image of the crystal-like aggregates grown at 65 °C for 1 week (0.25 mg/mL). The average aspect ratio amounts to 2.5 and the top ends clearly show facets at 125 degree angles. **C.** Aggregate 2D crystal lattice, the red line shows the 125° faceted top end for crystal-like aggregates and the black line a 90° strait top end (ribbon aggregates).
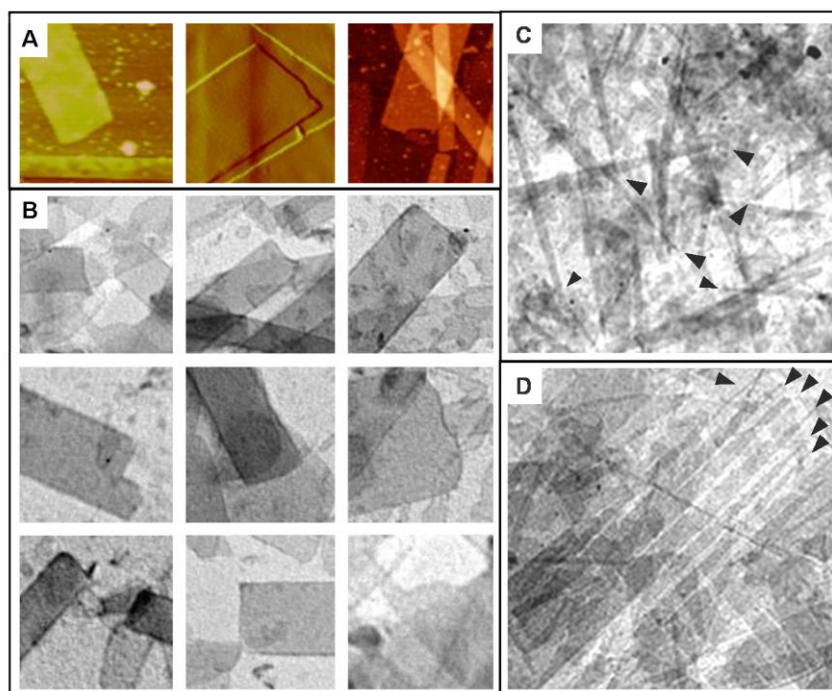
Figure S7. Roughening effects showing rounded, slanted, strait and unfinished top ends for **A.** images in AFM, **B.** TEM images. **C.** Single "dagger" shaped ribbons and **D.** many "dagger" shaped ends on a single broad ribbon characteristic of transport limited growth. (All aggregates were grown at a 0.25 mg/mL surfactant concentration and at temperatures below 55 °C.)
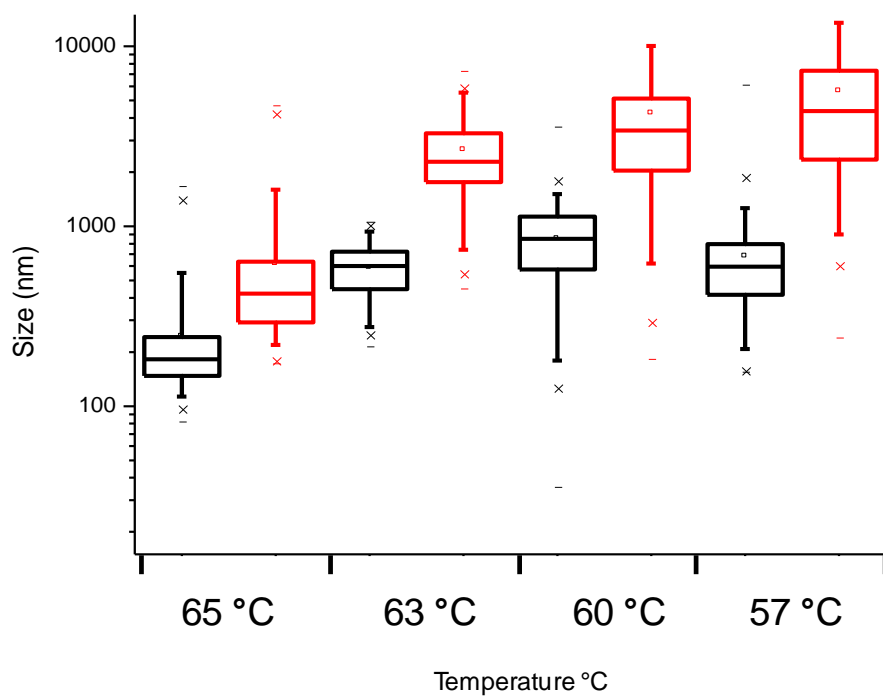
Figure S8. Log scaling of Figure 2A in the communication.
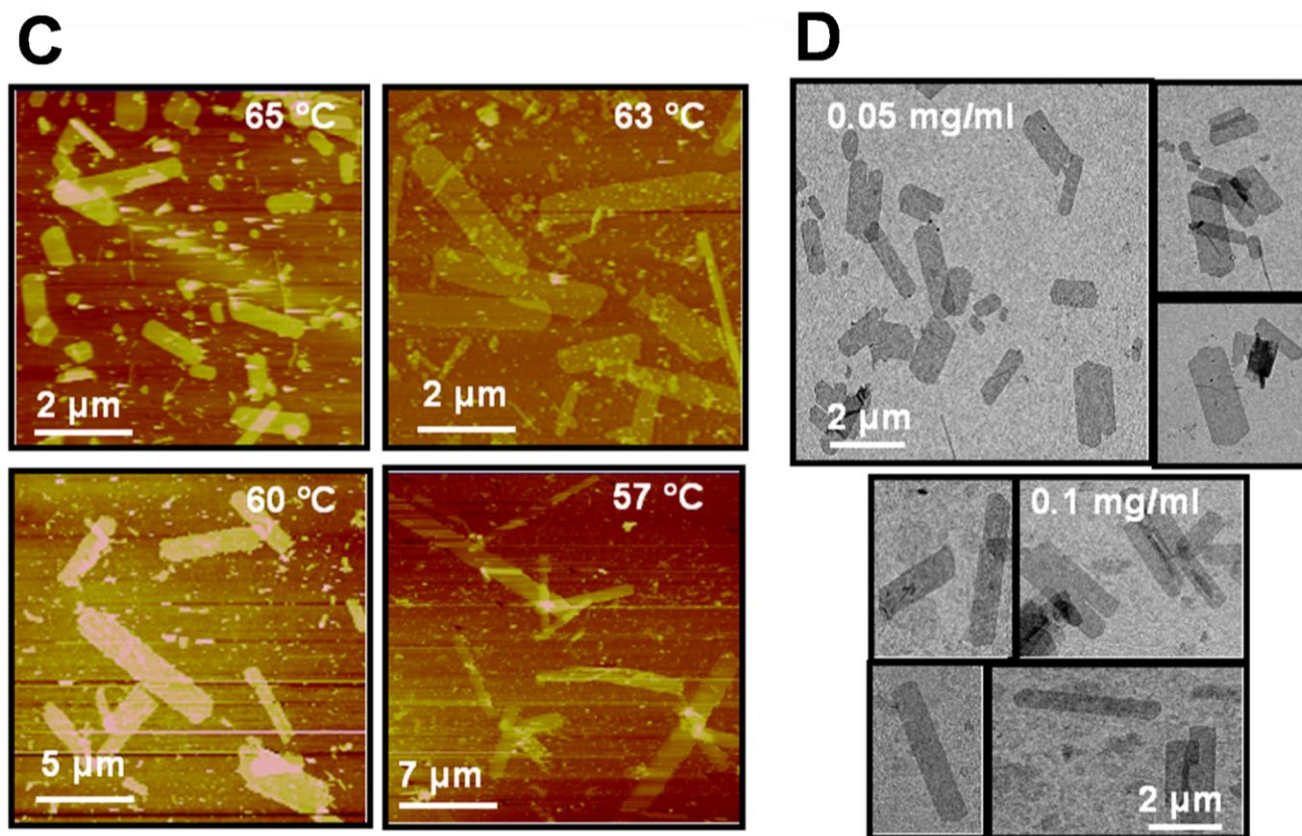
Figure S9. Enlarged images of figure 2C/D in the communication.

REFERENCES

1 Frederik, P. M.; Hubert, D. H. W. *Methods Enzymol.* **2005**, *391*, 431-448

2 Similar results were found for the β' polymorph of triacylglycerol crystals; F. F. Hollander, S. X. M. Boerrigter, J. van De Streek, R. F. P. Grimbergen, H. Meekes, P. Bennema, *J. Phys. Chem. B*, 1999, **103**, 8301

3 J. van Esch, R. M. Kellogg, B. L. Feringa, *Tetrahedron Lett*., 1997, **38**, 281; J. van Esch, F. Schoonbeek, M. de Loos, H. Kooijman, A. L. Spek, R. M. Kellogg, B. L. Feringa, *Chem. -Eur. J.*, 1999, **5**, 937; M de Loos, A. G. J. Ligtenbarg, J. van Esch, H. Kooijman, A. L. Spek, R. Hage, R. M. Kellogg, B. L. Feringa, *Eur. J. Org. Chem.*, 2000, 3675; M. C. Etter, Z. Urbanczyk-

Lipkowska, M. Zia-Ebrahimi, T. W. Panunto, *J. Am. Chem. Soc.*, 1990, **112**, 8415; A. J. Carr, R. Melendez, S. J. Geib, A. D. Hamilton, *Tetrahedron Lett.*, 1998, **39**, 7447.

4   For such a crystal plane at least one of the *hkl* indices should be 3. High indices crystal planes are almost never observed in crystal morphologies.

5   Grimbergen, R. F. P.; Meekes, H.; Bennema, P.; Strom, C. S.; Vogels, L. J. P. *Acta Crystallographica Section A: Foundations of Crystallography* **1998**, *54*, 491-500.

6   Hollander, F. F. A.; Boerrigter, S. X. M.; Van De Streek, J.; Grimbergen, R. F. P.; Meekes, H.; Bennema, P. *J. Phys. Chem. B* **1999**, *103*, 8301-8309.

7   Torchilin, V. P.; Levchenko, T. S.; Lukyanov, A. N.; Khaw, B. A.; Klibanov, A. L.; Rammohan, R.; Samokhin, G. P.; Whiteman, K. R. *Biochim. Biophys. Acta - Biomem.* **2001**, *1511*, 397-411.